JACS
JOURNAL OF THE AMERICAN CHEMICAL SOCIETY
Article
pubs.acs.org/JACS

Optimizing the Electronic Properties of Photoactive Anticancer Oxypyridine-Bridged Dirhodium(II,II) Complexes

Zhanyong Li,[†,⊥] Amanda David,[†,⊥] Bryan A. Albani,[‡] Jean-Philippe Pellois,*[,§] Claudia Turro,*[,‡] and Kim R. Dunbar*[,†]

[†]Department of Chemistry, Texas A&M University, College Station, Texas 77840, United States
[‡]Department of Chemistry and Biochemistry, The Ohio State University, Columbus, Ohio 43210, United States
[§]Department of Biochemistry & Biophysics, Texas A&M University, College Station, Texas 77843, United States

Supporting Information

ABSTRACT: A series of partial paddlewheel dirhodium compounds of general formula *cis*-$[Rh_2(xhp)_2(CH_3CN)_n][BF_4]_2$ (n = 5 or 6) were synthesized {xhp = 6-R-2-oxypyridine ligands, R = $-CH_3$ (mhp), $-F$ (fhp), $-Cl$ (chp)}. X-ray crystallographic studies indicate the aforementioned compounds contain two *cis*-oriented bridging xhp ligands, with the remaining sites being coordinated by CH_3CN ligands. The lability of the equatorial (eq) CH_3CN groups in these complexes in solution is in the order $-CH_3 > -Cl > -F$, in accord with the more electron rich bridging ligands exerting a stronger *trans* effect. In the case of *cis*-$[Rh_2(chp)_2(CH_3CN)_6][BF_4]_2$ (**5**), light irradiation enhances the production of the aqua adducts in which eq CH_3CN is replaced by H_2O molecules, whereas the formation of the aqua species for *cis*-$[Rh_2(fhp)_2(CH_3CN)_6][BF_4]_2$ (**7**) is only slightly increased by irradiation. The potential of both compounds to act as photochemotherapy agents was evaluated. A 16.4-fold increase in cytotoxicity against the HeLa cell line was observed for **5** upon 30 min irradiation (λ > 400 nm), in contrast to the nontoxic compound **7**, which is in accord with the results from the photochemistry. Furthermore, the cell death mechanism induced by **5** was determined to be apoptosis. These results clearly demonstrate the importance of tuning the ligand field around the dimetal center to maximize the photoreactivity and achieve the best photodynamic action.

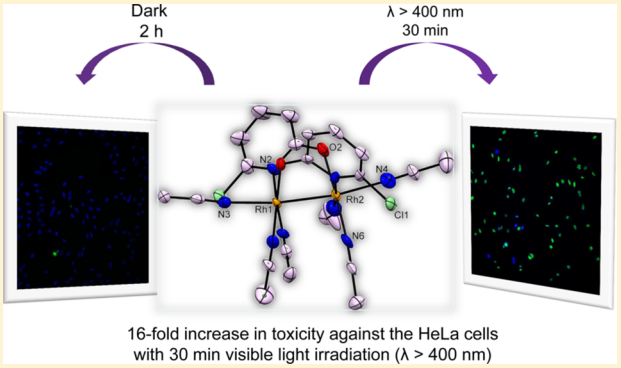

INTRODUCTION

The serendipitous discovery of the anticancer activity of cisplatin, *cis*-$Pt(NH_3)_2Cl_2$, and its approval by the U.S. Food and Drug Administration (FDA) for the treatment of testicular and ovarian cancers in 1978 launched a modern era of inorganic medicinal research.[1] It is well documented that the complex undergoes hydrolysis upon administration to generate the active aqua species *cis*-$[Pt(NH_3)_2Cl(H_2O)]^+$ and *cis*-$[Pt(NH_3)_2(H_2O)_2]^{2+}$, which preferentially bind to the N-7 guanine sites in DNA to form 1,2-intrastrand cross-links.[2−5] These lesions induce DNA distortions which result in the inhibition of transcription and DNA replication, ultimately leading to cell death.[2−5] In spite of the efficacy of cisplatin, severe nephrotoxicity as well as intrinsic and acquired resistance[6−8] have prompted the development of second- and third-generation platinum-based anticancer drugs. During the past three decades, only two other platinum drugs, namely carboplatin[9] and oxaliplatin,[10,11] have been approved for clinical use in the United States by the FDA, with several other platinum-based drugs being approved in other countries.[12] Although platinum-based anticancer agents are effective and represent the leading approaches to cancer therapy today,[13−16] there is a pressing need for the development of new drugs whose action is different than that of cisplatin to circumvent resistance issues as well as to find treatments for cancers that are unresponsive to Pt drugs. In this vein, transition-metal-containing complexes such as the families of dirhodium(II,II)[17] and dirhenium(III,III)[18] compounds, which are known to be potent anticancer active compounds, warrant further exploration.[19]

Photodynamic therapy (PDT) has emerged as a promising treatment for cancer and other malignancies, with several inherent advantages over conventional chemotherapy, including low levels of invasiveness and systematic toxicity because the active species are selectively generated in irradiated tissue.[20−24] The clinically approved drug for PDT treatment in the United States, Photofrin, functions by the production of $^1O_2$ (singlet oxygen) upon irradiation with visible light (~630 nm),[25] which leads to the generation of other reactive oxygen species. The reaction of these cytotoxic species damages tissue, leading to apoptosis and/or necrosis of cells in the affected area.[24] The low concentration of O_2, together with the need for diffusion of

Received: July 31, 2014
Published: December 1, 2014

   dx.doi.org/10.1021/ja5078359 | J. Am. Chem. Soc. 2014, 136, 17058−17070

O_2 from adjacent tissues once it is consumed during PDT, however, represent drawbacks and limit the effectiveness of these drugs in hypoxic tumors.[26−28] A different photochemotherapy (PCT) approach is the use of transition metal complexes which can, instead of producing $^1O_2$, bind covalently to relevant biomolecules upon irradiation due to the dissociation of photolabile ligands from a dissociative excited state, which represents an O_2-independent photochemical pathway.[29,30] Moreover, biologically active molecules can be attached to the metal complexes, as caged pro-drugs, as photolabile ligands that generate two active species—a metal complex with open coordination site(s) and free organic drug(s)—from a single precursor when activated with visible light.[31−33]

A recent study revealed the potential of the partial paddlewheel dirhodium(II,II) compound *cis*-$[Rh_2(O_2CCH_3)_2(CH_3CN)_6][BF_4]_2$ as a PCT agent (Scheme 1). It was

Scheme 1. Structural Representation of Photochemical Process for *cis*-$[Rh_2(O_2CCH_3)_2(CH_3CN)_6]^{2+}$ upon Visible Light Irradiation in H_2O

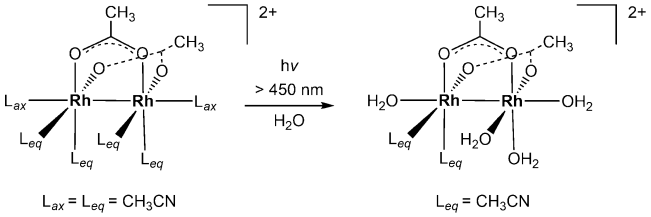

established in previous work that the photolability of the equatorial (eq) CH_3CN ligands, which are stable in the dark, is crucial for the formation of the active species upon irradiation with visible light.[34] As such, different dirhodium(II,II) complexes with photolabile CH_3CN ligands were developed by our research groups, including head-to-head (H-H) and head-to-tail (H-T) *cis*-$[Rh_2(NHOCCH_3)_2(CH_3CN)_6][BF_4]_2$[35] and unbridged $[Rh_2(phen)_2(CH_3CN)_6][BF_4]_4$ (phen = 1,10-phenanthroline),[36] which were found to exhibit promising potential as effective PCT anticancer agents. To better understand the relationship between the dark stability/photolability of the eq CH_3CN ligands in this type of partial paddlewheel dirhodium(II,II) complexes and their potential as PCT anticancer agents, substituted hydroxypyridine ligands were chosen as bridging ligands in the current study due to the opportunity for facile tuning of the ligand field in these complexes. The results detailed herein involve the syntheses and full characterization of a series of dirhodium(II,II) complexes featuring two *cis* 6-R-2-oxypyridinate (R = $-CH_3$, 6-methyl-2-oxypyridine, mhp; R = −Cl, 6-chloro-2-oxypyridine, chp; and R = −F, 6-fluoro-2-oxypyridine, fhp) bridging ligands. Moreover, the photochemistry of the synthesized compounds was investigated in a thorough fashion, the results of which are in good agreement with the cytotoxicity studies performed in HeLa cancer cells. More importantly, the current study highlights the critical role of tuning the ligation sphere of the dirhodium complexes to achieve optimal PCT action, which is accomplished by H-T *cis*-$[Rh_2(chp)_2(CH_3CN)_6][BF_4]_2$ (**5**) in this case.

EXPERIMENTAL SECTION

Materials. The compound $Rh_2(O_2CCH_3)_4{\cdot}2CH_3OH$ was either purchased from Pressure Chemical Co. or synthesized from $RhCl_3{\cdot}3H_2O$ as reported.[37] The ligands 6-methyl-2-hydroxypyridine (Hmhp) and 6-chloro-2-hydroxypyridine (Hchp) were purchased from Sigma-Aldrich and used as received; 6-fluoro-2-hydroxypyridine was purchased from VWR and used without further purification. The reagent Et_3OBF_4 (1.0 M in CH_2Cl_2) was purchased from Sigma-Aldrich. The solvents acetonitrile, dichloromethane, diethyl ether, chlorobenzene, dimethyl sulfoxide (DMSO), and tetrahydrofuran (THF) were of ACS grade and used as received. The NMR solvents D_2O (d_2), $CDCl_3$ (d), $(CD_3)_2CO$ (d_6), and CD_3CN (d_3) were purchased from Cambridge Isotope Laboratory. The compound $Rh_2(mhp)_4$ (**1**) was synthesized according to a slightly modified literature procedure.[38] Cell culture reagents Hoechst 33342, SYTOX green, and Annexin V-FITC were purchased from Invitrogen.

Syntheses. *Preparation of $Rh_2(chp)_4$ (**2**).* A quantity of ∼4.4 equiv of Hchp ligand (220 mg, 1.70 mmol) was mixed with a suspension of $Rh_2(O_2CCH_3)_4{\cdot}2CH_3OH$ (195 mg, 0.39 mmol) in 50 mL of chlorobenzene and refluxed for 36 h, which produced a pale green solution along with a large quantity of yellow precipitate. The solid was collected by filtration and then washed with copious volumes of CH_3OH (50 mL) to remove unreacted Hchp ligand. The yield is 235 mg, 85% based on rhodium. ^1H NMR ($CDCl_3$-d): δ 7.15 (dd, chp), 6.50 (dd, chp), 6.35(dd, chp).

*Preparation of $Rh_2(fhp)_4$ (**3**).* A quantity of ∼4.1 equiv of Hfhp ligand (186 mg, 1.65 mmol) was mixed with a suspension of $Rh_2(O_2CCH_3)_4{\cdot}2CH_3OH$ (200 mg, 0.40 mmol) in 50 mL of chlorobenzene and refluxed for 48 h. The resulting teal colored solution, which contained a large amount of green precipitate, was evaporated under vacuum, after which time 50 mL of CH_3OH was added. The solution was filtered through a medium frit to remove unreacted Hfhp ligand. The product was collected as a green solid (240 mg, 93% yield). Crystals suitable for X-ray diffraction were obtained from slow evaporation of an acetone solution containing the product in the presence of several drops of DMSO. ^1H NMR ($(CD_3)_2CO$-d_6): δ 7.29 (m, fhp), 6.22 (d, fhp), 6.09(d, fhp).

*Preparation of cis-$[Rh_2(mhp)_2(CH_3CN)_6][BF_4]_2$ (**4**).* An amount of $Rh_2(mhp)_4$ (81 mg, 0.13 mmol) was added to 30 mL of a mixture of CH_3CN/CH_2Cl_2 (v:v = 1:2). An aliquot of 0.5 mL of Et_3OBF_4 (1.0 M in CH_2Cl_2) was added to this suspension, leading to instantaneous formation of a clear green solution which eventually turned red over the course of 6 h. The solution was stirred at room temperature for 24 h and then concentrated to 5 mL. Treatment with 50 mL of diethyl ether led to precipitation of the product in an oily form. The oil was washed with copious quantities of diethyl ether and recrystallized by slow diffusion of diethyl ether into an acetonitrile solution of the product at room temperature. The yield is 82 mg, 75% based on rhodium. X-ray-quality crystals were obtained in a similar fashion. Elemental analysis calcd for $C_{24}H_{32}B_2N_8O_3F_8Rh_2$ (**4**·H_2O) (%): C, 33.52; H, 3.75; N, 13.03. Found: C, 33.61; H, 3.73; N, 12.84. ^1H NMR (CD_3CN-d_3): δ 7.21 (t, 2H, mhp), 6.36 (d, 2H, mhp), 6.22 (d, 2H, mhp), 2.63 (s, 6H, $-CH_3$ of mhp), 2.47 (s, 6H, eq CH_3CN *trans* to N), 2.46 (s, 6H, eq CH_3CN *trans* to O), 1.96 (s, free CH_3CN).

*Preparation of H-T (**5**) and H-H (**6**) Isomers of cis-$[Rh_2(chp)_2(CH_3CN)_6][BF_4]_2$.* An amount of $Rh_2(chp)_4$ (90.4 mg, 0.13 mmol) was suspended in 30 mL of CH_2Cl_2/CH_3CN (v:v = 1:2), and a 0.4 mL aliquot of Et_3OBF_4 (1.0 M in CH_2Cl_2) was then added to the flask. The solution gradually became clear over the course of the next 6 h, and stirring was continued at room temperature for a total of 28 h. The solution eventually became clear red and was concentrated to 5 mL. Treatment with 80 mL of diethyl ether led to the formation of an oily residue. The oil was washed with copious volumes of diethyl ether to obtain a red powder (98 mg). As evidenced by ^1H NMR spectroscopy, this solid contains both H-H and H-T isomers of *cis*-$[Rh_2(chp)_2(CH_3CN)_6][BF_4]_2$. The material was redissolved in 5 mL of CH_3CN, and slow diffusion of diethyl ether into this solution at −4 °C led to the crystallization of the H-T isomer. The yield is 50 mg, 44% based on rhodium. The crystals were collected by filtration, and the filtrate was condensed to 2 mL. Recrystallization of the H-H isomer was achieved by slow diffusion of diethyl ether into the CH_3CN solution at room temperature. The typical yield for the H-H isomer is much lower, ca. <10% for each batch of reaction. H-T isomer

dx.doi.org/10.1021/ja5078359 | J. Am. Chem. Soc. 2014, 136, 17058−17070

(**5**): Elemental analysis calcd for $C_{25}N_8O_4Cl_8H_{34}Rh_2B_2F_8$ ($\mathbf{5}\cdot 2H_2O\cdot 3CH_2Cl_2$) (%): C, 25.58; H, 2.92; N, 9.55. Found: C, 25.09; H, 2.67; N, 9.54. ^{1}H NMR (CD_3CN): δ 7.44 (t, 2H, chp), 6.71 (d, 2H, chp), 6.33 (d, 2H, chp), 2.57 (s, 6H, eq CH_3CN, *trans* to N), 2.38 (s, 6H, eq CH_3CN, *trans* to O), 1.96 (s, free CH_3CN). H-H isomer (**6**): ^{1}H NMR (CD_3CN-d_3): δ 7.38 (t, chp), 6.74 (d, chp), 6.57 (d, chp), 2.55 (s, eq CH_3CN, *trans* to N), 2.48 (s, eq CH_3CN, *trans* to O), 1.96 (free CH_3CN).

*Preparation of cis-[Rh$_2$(fhp)$_2$(CH$_3$CN)$_6$][BF$_4$]$_2$ (**7**).* An amount of $Rh_2(fhp)_4$ (184 mg, 0.28 mmol) was suspended in 30 mL of CH_3CN/CH_2Cl_2 (v:v = 1:1). An aliquot of 1.2 mL of Et_3OBF_4 (1.0 M CH_2Cl_2) was added, and the mixture was stirred for 4 days at room temperature. The initially turbid green mixture changed to a violet color and finally to red. The reaction solution was filtered to remove any insoluble materials, and the filtrate was concentrated to 5 mL. Treatment with 50 mL of diethyl ether led to precipitation of the desired product, which was washed with copious volumes of diethyl ether to obtain a red powder. The yield is 194 mg, 81%. Elemental analysis calcd for $C_{22}N_7O_6Cl_4H_{33}Rh_2B_2F_{10}$ ($7\cdot 4H_2O\cdot 2CH_2Cl_2$) (%): C, 25.15; H, 3.17; N, 9.33. Found: C, 25.03; H, 3.08; N, 9.57. ^{1}H NMR (CD_3CN-d_3): δ 7.49 (dd, fhp), 6.29(d, fhp), 6.21(d, fhp), 2.49 (eq CH_3CN, *trans* to N), 2.48 (eq CH_3CN, *trans* to O), 1.96 (free CH_3CN).

Physical Measurements. ^{1}H NMR spectroscopic data were collected on a 300 MHz Varian spectrometer. Chemical shifts in the spectra were referenced relative to the residual proton impurities of the deuterated solvent. Electronic absorption spectra were obtained on a Shimadzu UV-1601PC spectrometer. X-ray data sets for all the complexes were collected on a Bruker CCD APEX diffractometer with graphite-monochromated Mo Kα radiation (λ = 0.71073 Å). Cyclic voltammetric measurements were made using an H-CH Instruments analyzer and were performed at 298 K in dry CH_3CN with 0.1 M tetra-*n*-butylammonium hexafluorophosphate [*n*-Bu_4N][PF_6] as the supporting electrolyte. The $E_{1/2}$ values were referenced to the Ag/AgCl electrode without correction for the junction potentials [$E_{1/2}$ = $(E_{p,a} + E_{p,c})/2$]. The $FeCp_2/[FeCp_2]^+$ couple is located at $E_{1/2}$ = +0.45 V in CH_3CN at the same conditions used for the compounds. The working electrode was a glassy carbon electrode, the reference electrode was Ag/AgCl, and the counter electrode was a Pt wire. Elemental analyses were performed by Atlantic Microlab, Inc. The photolysis and quantum yield experiments were carried out using a 150 W Xe short arc lamp (USHIO) in a Milliarc lamp housing unit (PTI) powered by an LPS-220 power supply (PTI) equipped with an LPS-221 igniter (PTI) as the excitation source. The appropriate irradiation wavelengths were selected with a band-pass filter (Thorlabs, fwhm ≈ 10 nm) and long-pass filter (CVI Melles Griot). Electronic absorption spectroscopy for quantum yield measurements were performed using a Hewlett-Packard 8453 diode array spectrometer. The quantum yields (Φ) for photoinduced ligand exchange of CH_3CN in H_2O for **5** and **7** were measured with 400 nm irradiation. The rate of moles reacted at early irradiation times was quantitated using electronic absorption spectroscopy by monitoring the decrease in the metal-centered absorption band at 550 nm as a function of irradiation time (moles reacted/min). The photon flux of the Xe arc lamp (einsteins/min) with a 345 nm long-pass filter and a 400 nm band-pass filter was determined using ferrioxalate actinometry using standard methods.[39]

Theoretical Methods. The molecular and electronic structure calculations were performed by Density Functional Theory (DFT) methods using the Gaussian09 (G09) program package.[40] The MPW1PW91 correlation and exchange functionals[41] were used with the Stuttgart RSC 1997 Electron Core Potential (ECP)[42] basis set for the Rh atoms and the 6-31G(d′) basis set for the C, N, F, and H atoms.[43] Geometric parameters were taken from the crystal structures without the $[BF_4]^-$ anions and were used as the starting point for the simulations, followed by frequency calculations to evaluate the full optimization. Time-Dependent Density Functional Theory (TD-DFT)[44] calculations were conducted in the gas phase as well as using the polarized continuum model (PCM) with CH_3CN as the solvent.[45] The first 30 lowest singlet-to-singlet excitations were included in the TD-DFT calculations for both the gas-phase and solvation models studies. The molecular orbitals (MOs) were plotted by using the Agui graphical user interface[46] with an isovalue of 0.04, and the detailed analyses for the composition of the orbitals were obtained through the Chemissian program http://www.chemissian.com.

X-ray Crystallographic Methods. A hemisphere of data for **1**−**6** was collected by a combination of four sets of X-ray exposures. Each set used a different ϕ angle for the crystals and covered 0.5° in ω for **1**−**3**, 0.3° for **4**−**6**. The exposure times were 10 s for **1** and **2**, 20 s for **3**, **4**, and **6**, and 30 s for **5**. Crystal decay was monitored by analyzing duplicate reflections and was found to be less than 1%; therefore, no decay corrections were applied. The frames were integrated with the Bruker AXS SAINT Software package,[47] and the data were corrected for absorption using the SADABS program in the same software package.[48] The structures were solved and refined using X-SEED,[49] a graphical interface to SHELX2013.[50] In the final cycles of the refinement, all atoms except hydrogen atoms were refined anisotropically. The crystal parameters and information pertaining to the data collection and refinement of the crystals for **1** and **3**−**6** are summarized in Supporting Information, Table S1. Representative bond distances, angles, and dihedral angles are provided in the corresponding figure caption for each structure. The electron density corresponding to heavily disordered solvent molecules observed during the data refinement was removed using the SQUEEZE routine implemented in PLATON.

Cell Experiments. The HeLa cell line was obtained from the American Type Culture Collection, cell line CCL-2, and cells were cultured in Dulbecco's modified Eagle medium, containing 10% fetal bovine serum (Life Technologies), 50 μg/mL gentamicin, 4.5 mg/mL glucose, and 4 mM L-glutamine (Invitrogen Life Technology). Cell cultures were incubated in a humidified atmosphere containing 5% CO_2 at 37 °C.

For fluorescence microscopy imaging, the HeLa cells, at a concentration of 5000−10000 cell/μL, were harvested, 20 μL of cells were seeded in an eight-well sterile plate, and 180 μL of fresh medium was added to give a total volume of 200 μL. Cells were pre-incubated at 37 °C. After 48 h, the cells were washed three times with sterile PBS, and the medium was replaced by 200 μL of L-15 medium containing **5** or **7** at different concentrations. Plates were incubated for 2 h, after which time they were irradiated for 30 min in an LZC-4 UV/vis photoreactor, equipped with 14 UV lamps with wavelengths ranging from 300 to 450 nm. Eight-well sterile plates with 80% cell confluency in each well were placed on an inverted epifluorescence microscope (Model IX81, Olympus Center Valley, PA). The microscope is equipped with a heating stage, which was maintained at 37 °C. The microscope is configured with a spinning disk unit to perform both confocal and wide-field fluorescence microscopy. Images were captured with a Rolera-MGI Plus back-illuminated EMCCD camera (Qimaging, Surrey, BC, Canada). Imaging was performed using the fluorescence filter set FITC (Ex = 488 ± 10 nm/Em = 520 ± 20 nm) and CFP (Ex = 436 ± 10 nm/Em = 480 ± 20 nm).

The fluorescence intensities of HeLa cells were measured with the SlideBook 4.2 software (Olympus, Center Valley, PA). After irradiation for 30 min, the cells were treated with 10 μL of a 20 μM SYTOX Green solution and 4 μL of a 10 mg/mL solution of Hoechst 33342 and incubated for 10 min before imaging. Hoechst 33342 is a cell-permeable nucleic acid dye that stains the nucleus of all the cells, exhibiting blue fluorescence.[51,52] In order to determine if cells had a compromised plasma membrane after light irradiation inside the photochemical reactor, the cells were incubated with SYTOX Green. SYTOX Green is cell-impermeable and only stains cells with a compromised plasma membrane. For each experiment, six representative images were acquired using the 10× objective, and the percentages of dead cells were calculated from the ratio of cells stained by SYTOX Green divided by the number of cells stained by Hoechst 33342.

For the MitoProbe JC-1 Assay, the adherent cells (HeLa) were divided into four different groups and treated with compound **5** at the concentrations of 0 (control), 20, 50, and 75 μM, respectively. The experiment was initiated by incubating the cells with compound **5** for 2 h and then subjecting them to visible light irradiation for 30 min, after

which time an aliquot of 1 μL of JC-1 (2 μg/mL) solution was added to the cell culture. The time lapse experiment was performed with the 20 μM group for a total period of 3 h, with cell images being taken at different time intervals. For the control group, no compound was added to the cell culture. The cell imaging was performed using the fluorescence filter set FITC (Ex = 488 ± 10 nm/Em = 520 ± 20 nm) and RFP (Ex = 560 ± 20 nm/Em = 630 ± 35 nm), and the cells were imaged with a 10× objective.

To study the mechanism of cell death, cells were treated with Annexin V-FITC. The HeLa cells were incubated for 2 h with compound **5** at the LC_{50} concentration and then irradiated for 30 min in the UV photoreactor. The cells were washed with DPBS, and the medium was replaced with 200 μL of fresh L-15 media containing Annexin V-FITC. Cell imaging was performed using the 100× objective and the fluorescence filter set FITC.

RESULTS AND DISCUSSIONS

Syntheses and Characterization Studies. An excess of the Hmhp and Hchp ligands was used for the syntheses of **1** and **2**, respectively. After completion of the reactions, the unreacted ligands were removed by extraction with copious amount of CH_3OH, which led to the isolation of pure *trans*-(2,2) isomers, as evidenced by ^{1}H NMR spectra (Supporting Information, Figures S1 and S2, respectively) and X-ray crystallographic studies listed in the Supporting Information. The crystal structures of both complexes were published in previous reports, but the structure obtained herein for **1** exhibits unit cell parameters different from the published ones. Therefore, the detailed crystal data parameters are also provided in Table S1, along with the structural representation which is shown in Figure S3. Compound **3** was synthesized by a method different from the reported one and in improved yields.[53] Unlike the previously reported complex, it is only slightly soluble in THF, acetone, or ethanol. In the presence of several drops of DMSO, however, pale pink solutions containing **3** in THF, acetone, and ethanol were obtained. The X-ray crystallographic study revealed structural parameters slightly different from the previous ones; thus, the detailed data refinement and the graphic representation of the structure are shown in Table S1 and Figure S4, respectively.

NMR Spectral Studies. The alkylating agent Et_3OBF_4 was used to synthesize the partial paddlewheel complexes *cis*-$[Rh_2(xhp)_2(CH_3CN)_n][BF_4]_2$ (n = 5 or 6) (**4**–**7**, see Scheme 2), similar to the method adopted by Turro et al. to prepare H-H and H-T *cis*-$[Rh_2(HNOCCH_3)_2(CH_3CN)_6][BF_4]_2$.[34] The reaction between Et_3OBF_4 and **1** produces only one isomer, as indicated by its ^{1}H NMR (Supporting Information, Figure S5) spectrum, which was identified as the H-T isomer **4** by an X-ray crystallographic study (*vide infra*). The synthetic route adopted for *cis*-$[Rh_2(chp)_2(CH_3CN)_6][BF_4]_2$, however, resulted in the formation of both the H-H and H-T isomers, **5** and **6**, respectively, as indicated by ^{1}H NMR spectroscopy (Supporting Information, Figure S6). This finding indicates that the alkylating agent Et_3OBF_4 does not react discriminately with the two chp ligands in the *cis* positions of the *trans*-(2,2) starting material, which would be expected to lead only to the formation of **5**, but also with the two bridging ligands occupying the *trans* positions. The resulting *trans*-H-H $[Rh_2(chp)_2(CH_3CN)_6][BF_4]_2$ product must then undergo rearrangement into the more stable *cis* isomer to produce compound **6**. Compound **7**, the ^{1}H NMR spectrum of which is provided in Supporting Information, Figure S7, was synthesized by a procedure similar to the one used for complexes **4** and **5** but with much longer reaction times due to the low solubility of **3** in the solvent used. Many trials to obtain a single crystal of compound **7** were unsuccessful. From the structure of precursor **3** (isomer (4,0)-$Rh_2(fhp)_4$, determined crystallographically, Figure S4, and by ^{1}H NMR spectroscopy), however, we can conclude that compound **7** adopts the H-H configuration.

Scheme 2. General Synthetic Procedure for Complexes 4–7

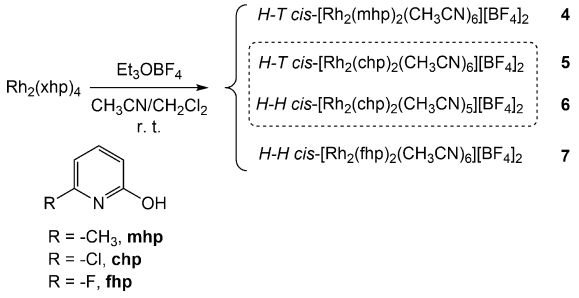

As shown in Supporting Information, Figure S8, three different resonances in the aliphatic region are present in the ^{1}H NMR spectrum of **4** collected ∼2 min after dissolution in CD_3CN, with chemical shifts of 2.63, 2.47, and 2.46 ppm, respectively. The peak at ∼2.63 ppm is assigned to the $-CH_3$ groups on the mhp ligands since its intensity does not change over the course of the experiment. The other two closely spaced resonances are attributed to the two different sets of eq CH_3CN ligands, which are *trans* to the O and N atoms of the mhp ligands, respectively. After 15 min, a distinct decrease in intensity for the resonance at ∼2.47 ppm and an increase at 1.96 ppm for free CH_3CN are observed, attributed to fast exchange with the CD_3CN molecules. The 2.47 ppm feature disappeared after 75 min in the dark, indicating the much faster exchange process with the CD_3CN molecules than that in *cis*-$[Rh_2(O_2CCH_3)_2(CH_3CN)_6][BF_4]_2$.[33] At this stage, two of the eq CH_3CN ligands have exchanged with the CD_3CN molecules, as judged by the integration data. The sample was kept in the dark for a longer period of time, and the subsequently obtained spectra indicate that exchange with the CD_3CN molecules for the resonance at 2.46 ppm also takes place, albeit at a much slower rate, resulting in a final integration corresponding to 5 equiv of free CH_3CN after 23 h.

An investigation of the lability of the eq CH_3CN ligands in compound **5** was conducted in a similar fashion. In this case, two resonances at 2.57 and 2.38 ppm are observed, corresponding to the eq CH_3CN ligands *trans* to the N and O atoms of the chp ligand, respectively. As shown in Supporting Information, Figure S9, the intensities of both peaks decrease simultaneously, with the exchange rate for the latter resonance being faster than that for the former one. Both exchange processes are much slower, however, than that of compound **4**, presumably due to the weaker *trans* effect exerted by bridging chp ligands owing to the presence of electron-withdrawing Cl substituents in **5**.

For compound **7**, the two types of eq CH_3CN ligands, namely either *trans* to the N or to the O atoms of the fhp ligands, exhibit only slightly different chemical shifts (δ = 2.49 and 2.48 ppm). The former resonance disappears over a period of ∼340 h, indicating its complete substitution by CD_3CN molecules, whereas the latter one has only negligible changes in intensity during the same period of time (Supporting Information, Figure S10). These features are ascribed to the

dx.doi.org/10.1021/ja5078359 | J. Am. Chem. Soc. 2014, 136, 17058–17070

much stronger electron-withdrawing ability of the F substituents on the bridging fhp ligands.

The exchange of eq CH_3CN with D_2O solvent molecules in **4** was also monitored by ^1H NMR spectroscopy in the dark. Upon dissolution in D_2O, the solution turns green, in contrast to its red color in CD_3CN. A very fast substitution process involving the D_2O molecules is apparently occurring, a fact that is supported by the complicated ^1H NMR spectrum and the one intense signal at 2.06 ppm from free CH_3CN (Supporting Information, Figure S11). Similarly, for both compounds **5** and **7**, there is also exchange of eq CH_3CN ligands with D_2O molecules in the dark, but this occurs at a significantly slower rate as compared to that in **4** (Supporting Information, Figures S12 and S13, respectively). This observation is also in accord with the results from the electronic absorption spectroscopic studies on **5** and **7** in H_2O in the dark (Supporting Information, Figure S14).

X-ray Crystallographic Studies. Crystallographic parameters for compounds **4**–**6** are provided in Table S1 in the Supporting Information.

cis-$[Rh_2(mhp)_2(CH_3CN)_6][BF_4]_2$ **(*4*).** The compound crystallizes in the chiral space group $P2_12_12_1$. The dirhodium cation contains two *cis* bridging mhp ligands arranged in a H-T fashion. Six CH_3CN ligands complete the pseudo-octahedral coordination sphere of the central rhodium units (Figure 1),

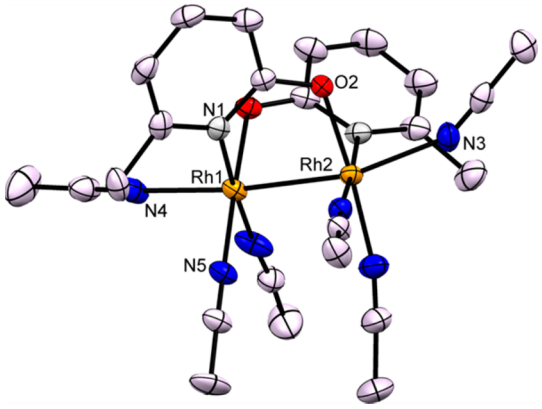

Figure 1. Thermal ellipsoid plot of the cationic part of compound **4** at the 50% probability level. Anions and hydrogen atoms are omitted for the sake of clarity. Representative bond distances and dihedral angles are as follows: Rh1–Rh2 2.4793(7), Rh1–O1 2.007(4), Rh1–N1 2.057(5), Rh1–N5 1.999(5), Rh1–N4 2.201(5); N1–Rh1–Rh2–O2 −30.8(2), N5–Rh1–Rh2–N7 −36.5(2). Colors for thermal ellipsoids: Rh, orange; N, blue; C, pink; O, red.

and there are two $[BF_4]^-$ counterions. One of the eq CH_3CN ligands and a $[BF_4]^-$ counterion are disordered between two different positions with site occupancies of 0.6366/0.3634 and 0.3765/0.6235, respectively. Racemic twinning was refined during the last cycle, with the Flack parameter of 0 and an esd value of 0.9416. The Rh–Rh bond distance is 2.4793(7) Å, which is ∼0.12 Å longer than that observed for **1**, which we ascribe to the less sterically demanding mhp ligands in **4**. The Rh–N (ax CH_3CN) bond distances are 2.234(5) and 2.201(5) Å, significantly longer than the Rh–N (eq CH_3CN) bond distances, which are in the range of 1.999(5)–2.014(5) Å. The Rh–N (mhp) and Rh–O (mhp) bond distances are comparable to the corresponding distances in **1**. The distortions of the eq CH_3CN and mhp ligands away from the eclipsed confirmation reflect repulsive effects. The dihedral angles defined by N5–Rh1–Rh2–N7 and N6–Rh1–Rh2–N8 are −36.5(1)° and −36.9(2)°, respectively, larger than those in *cis-*$[Rh_2(DTolF)_2(CH_3CN)_6][BF_4]_2$, *cis-*$[Rh_2(F\text{-}form)_2(CH_3CN)_6][BF_4]_2$, and *cis-*$[Rh_2(DTolF)_2(dppz)_2(CH_3CN)][BF_4]_2$.[54,55] Slightly smaller distortions are observed for the two mhp bridging ligands, with the dihedral angles defined by O1–Rh1–Rh2–N2 and N1–Rh1–Rh2–O2 being −30.3(2)° and −30.8(2)°, respectively.

H-T cis-$[Rh_2(chp)_2(CH_3CN)_6][BF_4]_2{\cdot}CH_3CN$ **(*5*·CH_3CN).** Compound **5** crystallizes in the space group $P2_1/c$ with a coordination sphere similar to that of compound **4**, as can be seen in Figure 2. One of the eq CH_3CN ligands is disordered

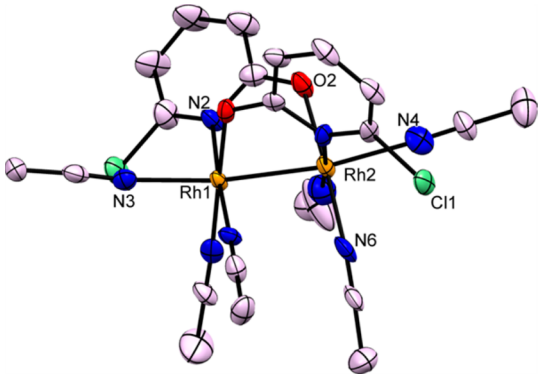

Figure 2. Thermal ellipsoid plot of the cationic part of compound **5** at the 50% probability level. Anions and hydrogen atoms are omitted for the sake of clarity. Important bond distances (Å) and dihedral angles (deg) are as follows: Rh1–Rh2 2.492(1), Rh1–N3 2.21(1), Rh1–O1 2.005(6), Rh1–N7 1.987(9), Rh1–N2 2.071(8), Rh1–N8 2.030(9), Rh2–N4 2.25(1); O1–Rh1–Rh2–N1 30.9(3), N7–Rh1–Rh2–N5 37.6(4). Colors for thermal ellipsoids: Rh, orange; N, blue; C, pink; O, red; Cl, light green.

over two positions with site occupancies of 0.5203/0.4797. The Rh–Rh bond distance is 2.492(1) Å in **5**, ∼0.11 Å longer than that of compound **2** because there are fewer constraints from the two bridging ligands in **5**, as compared to four of them in **2**. The Rh–N (ax CH_3CN) bond distances are 2.21(1) and 2.25(1) Å, longer than the Rh–N (eq CH_3CN) bond distances which range from 1.97(1) to 2.030(9) Å. Similar distortions from the eclipsed configuration of the eq CH_3CN ligands occur, with larger distortions for the eq CH_3CN ligands than those defined by the chp ligand.

H-H cis-$[Rh_2(chp)_2(CH_3CN)_5](BF_4)_2{\cdot}2CH_3CN$ **(*6*).** Compound **6** crystallizes in the space group $P\bar{1}$. The thermal ellipsoid plot of the cationic unit (Figure 3) consists of two *cis* bridging chp ligands in a H-H fashion, four eq CH_3CN ligands, and one axial (ax) CH_3CN molecule coordinated to the Rh center that is bonded to the O atoms of the bridging chp ligands. The Rh–Rh bond distance is 2.506(1) Å, slightly longer than those in **4** and **5**. The Rh–N (ax CH_3CN) bond distance is 2.115(2) Å, ∼0.1 Å shorter than those in **4**, **5**, and H-T *cis-*$[Rh_2(HNOCCH_3)_2(CH_3CN)_6][BF_4]_2$.[34] The Rh–N (eq CH_3CN) bond distances fall in a small range of 1.991(3)–2.002(2) Å, similar to those in **4** and **5**. Much smaller distortions from the eclipsed configuration defined by the eq CH_3CN ligands in **6** occur as compared to those found for **4** and **5**, with the dihedral angles defined by N4–Rh1–Rh2–N6 and N3–Rh1–Rh2–N5 being 23.5(1)° and 23.53(9)°, respectively. Distortions of the bridging chp ligands are only slightly smaller, with the angles being 19.39(9)° and 21.75(8)°, respectively.

dx.doi.org/10.1021/ja5078359 | J. Am. Chem. Soc. 2014, 136, 17058–17070

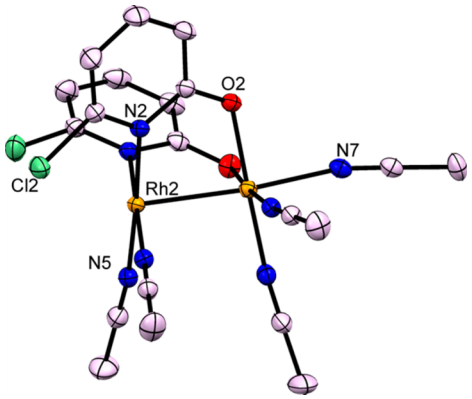

Figure 3. Thermal ellipsoid plot of the cationic part of compound **6** at the 50% probability level. Anions and hydrogen atoms are omitted for the sake of clarity. Representative bond distances (Å) and dihedral angles (deg) are as follows: Rh1−Rh2 2.506(1), Rh2−N1 2.034(3), Rh1−O2 2.001(2), Rh1−N7 2.115(2), Rh2−N6 2.002(2), N2−Rh1−Rh2−O2 −21.75(8), N3−Rh1−Rh2−N5 23.53(9). Colors for thermal ellipsoids: Rh, orange; N, blue; C, pink; O, red; Cl, light green.

Electronic Absorption Spectroscopic and Electrochemical Studies. The electronic absorption spectra of **5** and **7** were measured at room temperature in H_2O, and their photophysical data are summarized in Table 1.

Table 1. Photophysical Properties of 4, 5, and 7 in H_2O at Room Temperature

	λ/nm ($\varepsilon \times 10^3$/M^{-1}·cm^{-1})
4	239 (36.9), 259 (29.0), 303 (6.0), ~389 (0.78), 498 (0.20)[a]
5	236 (20.0), 259 (17.4), 302 (3.4), 381 (0.37), 550 (0.12)
7	226 (35.9), 257 (33.5), 294 (4.8), 397 (0.47), 558 (0.18)

[a]In CH_3CN.

Compounds **5** and **7** exhibit similar electronic absorption spectroscopic properties in H_2O at room temperature. It was not possible to obtain the spectrum of **4** in H_2O, however, due to the fast exchange of eq CH_3CN with H_2O solvent molecules, as evidenced by ^{1}H NMR spectroscopy (*vide supra*). The transitions at $\lambda \approx 550$ nm in **5** and $\lambda \approx 558$ nm in **7** have very similar low molar absorptivities (Table 1). They are tentatively assigned as the $Rh_2(\pi^*) \rightarrow Rh_2(\sigma^*)$ metal-centered (MC) bands, similar to other documented dirhodium complexes,[56] but a minor contribution from ligand-to-metal charge-transfer (LMCT) character is expected due to the dependence of the maximum on the bridging ligands. Another weak but distinct feature of this series of compounds is the absorption in the region of 380−400 nm, similar to the transitions at ~350 nm for both the H-H and H-T isomers of *cis*-$[Rh_2(HNOCCH_3)_2(CH_3CN)_6][BF_4]_2$[34] and the transition at ~363 nm in *cis*-$[Rh_2(O_2CCH_3)_2(CH_3CN)_6][BF_4]_2$.[33] These features are ascribed to combinations of electronic transitions from the filled $Rh_2(\pi^*)$ orbitals to Rh-eq $CH_3CN(\sigma^*)$ and $Rh_2(\sigma^*)$ unoccupied orbitals. As shown in Table 1 and Figure 4, medium absorption features at ~290−300 nm are also present in all three compounds. Due to the independence of the energies on the bridging ligands, these bands are assigned as MC transitions originating from $Rh_2(\pi)$ and $Rh_2(\sigma)$ to Rh-eq $CH_3CN(\sigma^*)$ and $Rh_2(\sigma^*)$ orbitals, respectively.

For the sake of comparison, electronic absorption spectra of **4**−**7** were also measured in CH_3CN (Supporting Information, Figure S15 and Table S2). A slight hypsochromic shift of the lowest energy transition was observed for both **5** and **7** in CH_3CN as compared to the corresponding maxima in aqueous solutions (Table S2). This result is similar to that reported for the spectral shift for *cis*-$[Rh_2(O_2CCH_3)_2(CH_3CN)_6][BF_4]_2$ in CH_3CN as compared to H_2O and is consistent with the partial charge-transfer character of this band.[33] In contrast, the transitions of **5** and **7** in the 200−390 nm range exhibit negligible shifts from CH_3CN to H_2O, in accord with the involvement of only MC orbitals and those from the eq CH_3CN ligands.

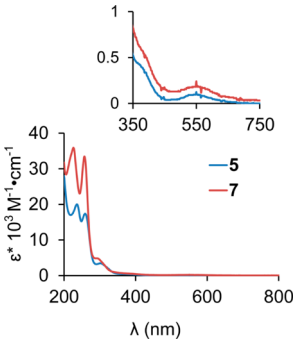

Figure 4. Electronic absorption spectra of compounds **5** and **7** obtained in H_2O at room temperature.

The electrochemical data for compounds **1**−**5** and **7**, as well as the free ligands Hmhp, Hchp, and Hfhp, are compiled in Table 2. The strong electron-donating ability of the mhp ligands renders the dimetal center electron-rich, thus leading to a cathodic shift of the first oxidation potential by ~+0.30 V in **1** as compared to that in $Rh_2(O_2CCH_3)_4$. On the other hand, this couple is observed at a more positive potential ~+1.23 V in **2**, most likely due to the electron-withdrawing Cl atoms on the bridging chp groups. Both **1** and **2** exhibit one reversible reduction at −1.36 and −1.20 V, respectively, attributed to the Rh_2^{4+}/Rh_2^{3+} redox couple. The less accessible reduction for **1** is also in accord with the electron-donating $-CH_3$ groups, resulting in an electron-rich dimetal core. Complex **3** exhibits different electrochemical properties as compared to **1** and **2**, presumably because of the different ligand configuration. It exhibits one irreversible reduction at ~−1.49 V, one irreversible oxidation at ~+0.99 V, and another quasi-reversible oxidation at ~+1.20 V. There are two irreversible reduction processes for **4** and three irreversible reductions for **5** and **7**. The two reduction processes for **4**, the first two for **5**, and the first and third ones for **7** are ascribed to stepwise reductions of the dimetal center, namely the Rh_2^{4+}/Rh_2^{3+} and Rh_2^{3+}/Rh_2^{2+} redox couples, respectively. The third reduction in **5** and the second reduction in **7** are tentatively assigned as bridging-ligand-based redox events, since similar features occur for the free Hchp and Hfhp ligands at −1.44 and −0.92 V, respectively. One quasi-reversible oxidation appears for **4** and two for **7**, tentatively assigned as a MC oxidation, but with contributions from the bridging ligands, unlike the case of **5**.

Computational Studies. To aid in the interpretation of the electronic structures of **4**, **5**, and **7**, computational studies of their cationic units were conducted. For **4** and **5**, the gas-phase optimizations began with the cationic units taken directly from the respective crystal structures, whereas for **7** the cationic unit was built in "agui" by modification of the crystal structure for **6** but with both axial positions occupied by CH_3CN ligands. The calculated structures are very similar to those determined

dx.doi.org/10.1021/ja5078359 | J. Am. Chem. Soc. 2014, 136, 17058−17070

Table 2. Electrochemical Data of Complexes 1−5 and 7 as Well as the Free Ligands Hmhp, Hchp, and Hfhp (V vs Ag/AgCl, 0.1 M [*n*-Bu_4N][PF_6], 0.2 V/s)

	$E_{pc,1}$	$E_{pc,2}$	$E_{pc,3}$	$E_{ox,1}$	$E_{ox,2}$
Hmhp				1.51[a]	
Hchp	−1.03	−1.44		1.85[a]	
Hfhp	−0.92				
$Rh_2(mhp)_4$ (**1**)[b]	−1.36[c]			0.91	
$Rh_2(chp)_4$ (**2**)[d]	−1.20[c]			1.23	
$Rh_2(fhp)_4$ (**3**)[d]	−1.49			0.99[a]	1.20[c]
cis-$[Rh_2(mhp)_2(CH_3CN)_6][BF_4]_2$ (**4**)	−0.45	−1.27		1.61[e]	
cis-$[Rh_2(chp)_2(CH_3CN)_6][BF_4]_2$ (**5**)	−0.24	−1.13	−1.44		
cis-$[Rh_2(fhp)_2(CH_3CN)_6][BF_4]_2$ (**7**)	−0.66	−1.18	−1.34	1.27[e]	1.48[e]

[a]Irreversible. [b]In CH_2Cl_2. [c]Reversible. [d]In CH_3CN, with the presence of drops of DMSO. [e]Quasi-reversible.

experimentally for both **4** and **5**, indicating the accuracy of the levels of theory and the basis sets chosen. The graphic representations of the calculated structures are displayed in Supporting Information, Figure S16, and the important calculated structural parameters are summarized in Supporting Information, Table S3. TD-DFT calculations using both CH_3CN and H_2O as solvents were based on the gas-phase optimized structures. One issue that needs to be pointed out is that, due to the lability of the ax CH_3CN upon dissolution in H_2O, the TD-DFT calculations in H_2O were started from the optimized *cis*-$[Rh_2(chp)_2(CH_3CN)_4{\cdot}2H_2O]^{2+}$ and *cis*-$[Rh_2(fhp)_2(CH_3CN)_4{\cdot}2H_2O]^{2+}$ for **5** and **7**, respectively.

The electron densities on the HOMO and HOMO−1 orbitals are mainly concentrated on the respective bridging ligand (mhp in **4**, chp in **5**, and fhp in **7**), with ∼75% ligand character in the HOMO and ∼85% in the HOMO−1, whereas the orbitals ranging from the HOMO−2 to HOMO−8 are mainly MC (Supporting Information, Table S4, and Figure 5).

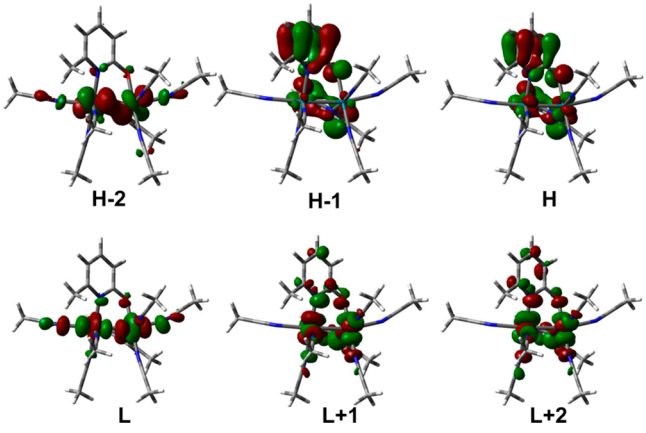

Figure 5. MO visualizations of **4** in the solvation model with CH_3CN as the solvent, generated by Agui[46] with isovalue = 0.04; H = HOMO, L = LUMO.

For the unoccupied orbitals, the LUMO is mainly rhodium-based and has $Rh_2(\sigma^*)$ character clearly evident in the visualization. The LUMO+1 and LUMO+2 have significant σ^* anti-bonding interactions between the Rh and the eq CH_3CN ligands (Figure 5). The results obtained from the DFT calculations using H_2O as the solvent indicate the MO compositions in compounds **4**, **5**, and **7** are similar to those calculated in CH_3CN (Supporting Information, Table S5).

As shown in the MO diagrams provided in Figure 6, all of the calculated orbitals in **5** lie at slightly lower energies than the

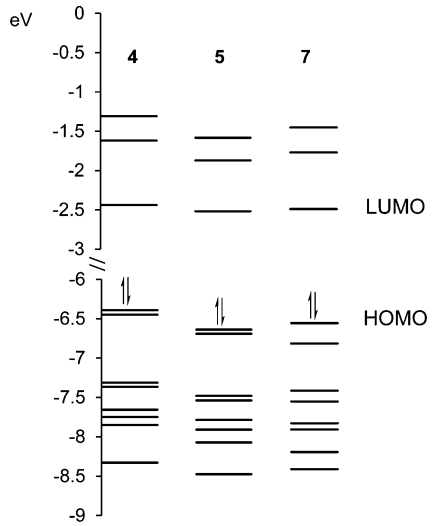

Figure 6. Calculated MO diagrams of **4**, **5**, and **7** using CH_3CN as the solvent with selected orbital contributions listed in Table S4.

corresponding MOs in **4**. This difference can be explained by the stabilization caused by the electron-withdrawing bridging ligands (Table S4), although different degrees of stabilization occur for each orbital pair because of the varying contributions from the bridging ligands. For example, the HOMO in **5** is ∼0.25 eV lower in energy than that in **4**, while the stabilization of the LUMO is only ∼0.08 eV, resulting in a larger HOMO−LUMO gap in **5** as compared to **4**. For compound **7**, the composition of each MO is very similar to those of the corresponding orbitals in **4** and **5** as shown in Table S4; however, no trend was observed for the energy of each orbital when compared to those in the former, probably due to the H-H orientation of the two bridging fhp ligands. Nevertheless, the HOMO−LUMO gap of **7** was predicted to be ∼0.05 eV smaller than that in **5**, ∼0.12 eV larger than that in **4**.

Based on the TD-DFT calculations, the lowest energy absorption band for each complex corresponds to transitions from the HOMO and HOMO−3 to the LUMO, as shown in Supporting Information, Tables S6−S8, such that they possess both MC and MLCT character. These transition energies are predicted to lie at 485, 462, and 473 nm for **4**, **5**, and **7**, respectively, which are in good agreement with the experimental data (Tables 1 and S2). The absorption bands ∼380−400 nm in all three compounds were predicted to be the transitions to the LUMO+1 [Rh-eq $CH_3CN(\sigma^*)$ character], which may be involved in dissociation of the eq CH_3CN upon irradiation in this wavelength range. Of particular note is that

dx.doi.org/10.1021/ja5078359 | J. Am. Chem. Soc. 2014, 136, 17058−17070

the lowest energy band in each complex in H_2O exhibits a bathochromic shift as compared to those in CH_3CN, also consistent with the experimental data (Tables 1 and S2) as well as our previous findings.[33,34]

Photochemistry. It was reported by Turro et al. that, upon visible light irradiation, two of the eq CH_3CN molecules exchange with H_2O molecules in *cis*-$[Rh_2(O_2CCH_3)_2(CH_3CN)_6][BF_4]_2$ as well as in the H-H and H-T isomers of *cis*-$[Rh_2(NHCOCH_3)_2(CH_3CN)_6][BF_4]_2$ in aqueous solutions. Therefore, compounds **5** and **7** were selected for further photochemical experiments due to their relative stability in water in the dark. Both complexes are expected to undergo excited-state reactivity similar to that of *cis*-$[Rh_2(O_2CCH_3)_2(CH_3CN)_6][BF_4]_2$ upon irradiation with visible light, for which the exchange of the eq CH_3CN for H_2O molecules was reported. The changes in the electronic absorption spectrum of **5** as a function of irradiation time are displayed in Figure 7a,

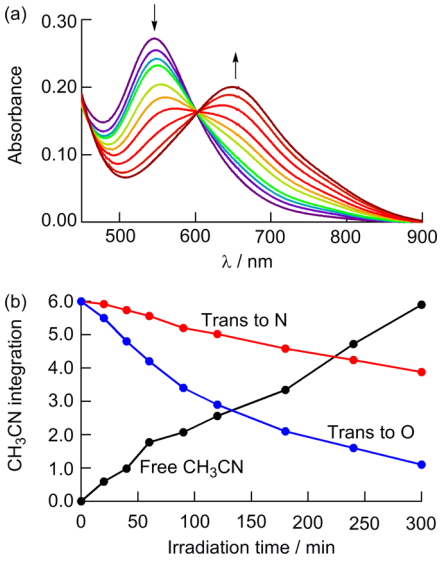

Figure 7. Photolysis of **5** (a) in water monitored through changes in the electronic absorption spectrum (0−300 min, $\lambda_{irr} \geq 395$ nm), and (b) in CD_3CN showing the changes in the integration of the ^1H NMR signals of the eq CH_3CN peaks at 2.38 ppm (*trans* to O) and 2.57 ppm (*trans* to N), and free CH_3CN ($\lambda_{irr} \geq 395$ nm).

which shows a shift in the maximum of the lowest energy band from 550 to 615 nm upon irradiation with an isosbestic point at 602 nm. Similar bathochromic shifts were reported for the related complexes *cis*-$[Rh_2(O_2CCH_3)(CH_3CN)_6][BF_4]_2$ and *cis*-$[Rh_2(NHCOCH_3)_2(CH_3CN)_6][BF_4]_2$, both of which undergo photoinduced exchange of eq CH_3CN ligands for solvent H_2O molecules.[33,34] ^1H NMR studies were undertaken with **5** and **7** in CD_3CN and D_2O in order to ascertain the identity of the photochemical products in each solvent.

Changes in the ^1H NMR spectrum of **5** as a function of irradiation time in CD_3CN are shown in Supporting Information, Figure S17; the integration of the peaks at 2.38 and 2.57 ppm, which correspond to eq CH_3CN ligands positioned *trans* to the O and N atoms of the chp bridging ligand, respectively, during the photolysis is displayed in Figure 7b. It is evident from the data in Figures 7b and S17 that the initial spectrum contains two resonances at 2.38 and 2.57 ppm of equal intensity. In addition, free CH_3CN ligand is also observed in the spectrum at $t = 0$ min (Figure S17), consistent with the known facile exchange of the axial ligands in coordinating solvents.[33,34] Irradiation of the solution with $\lambda_{irr} \geq 395$ nm reveals the exchange of both types of eq CH_3CN ligands with CD_3CN solvent molecules; however, those positioned *trans* to O atoms (δ = 2.38 ppm) of the bridging ligand exhibit ~3.4-fold greater photolability than those positioned *trans* to N chp atoms (δ = 2.57 ppm), as determined from the slopes of the plots in Figure 7b from 0 to 120 min (at later irradiation times, the product present in solution absorbs a significant portion of the excitation photons, making the overall reaction slower). The increased photoinduced exchange of the eq CH_3CN ligands *trans* to the oxygen atom, as compared to those *trans* to the nitrogen atom, is consistent with the previous findings reported for H-T *cis*-$[Rh_2(NHCOCH_3)_2(CH_3CN)_6][BF_4]_2$.[34] An important point to note is that this photochemistry also takes place with $\lambda_{irr} \geq 645$ nm; however, the irradiation times required are significantly longer owing to the lower number of photons absorbed by the molecule relative to $\lambda_{irr} \geq 395$ nm.

Similar results are observed for the photolysis of **5** in D_2O, but in this case the product resulting from the exchange of one eq CH_3CN ligand, positioned *trans* to either a N or O atom of chp, to form H-T *cis*-$[Rh_2(chp)_2(D_2O)(CH_3CN)_3\cdot(D_2O_{ax})_2][BF_4]_2$ gives rise to three new CH_3CN resonances (Figure 8). As depicted in Figure 8, the peaks at 2.66 (CH_3CN *trans* to N, CH_3CN^N) and 2.44 ppm (CH_3CN *trans* to O, CH_3CN^O) in **5** decrease in intensity, with concomitant growth of the resonance at 2.06 ppm (†), corresponding to free CH_3CN. These changes are accompanied by the appearance of three new peaks at early

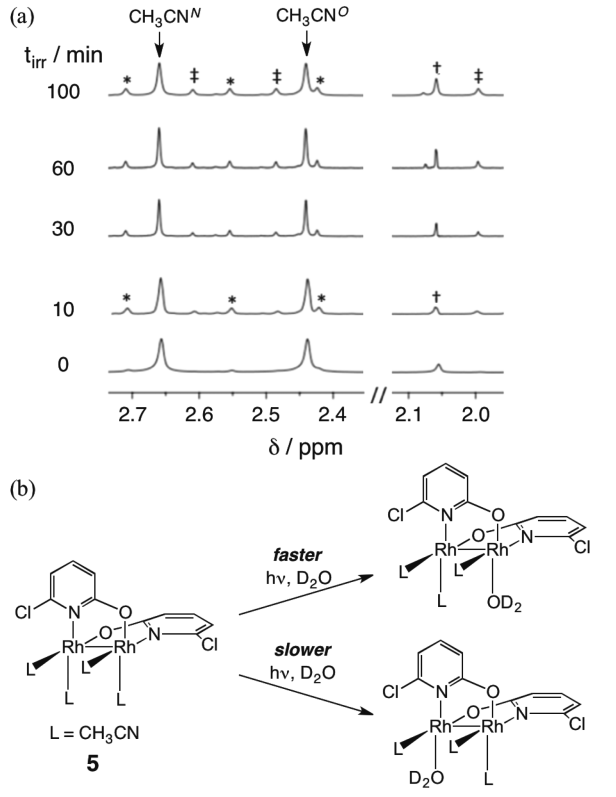

Figure 8. (a) Changes in the ^1H NMR spectra of **5** as a function of irradiation time in D_2O ($\lambda_{irr} \geq 395$ nm), where CH_3CN^N and CH_3CN^O represent the eq CH_3CN ligands positioned *trans* to the chp N and O atom, respectively; † is free CH_3CN, and * and ‡ are resonances associated with two different mono-aqua products. (b) Schematic representation of the formation of the two photoproducts.

dx.doi.org/10.1021/ja5078359 | J. Am. Chem. Soc. 2014, 136, 17058−17070

irradiation times (10 min), labeled with an asterisk (*) in Figure 8a, at 2.43, 2.56, and 2.72 ppm. On the basis of the results obtained in CD_3CN, as well as those previously reported for the analogous $NHCOCH_3$-bridged complex,[34] it is believed that the photoinduced exchange of the eq CH_3CN ligands positioned *trans* to the chp O atoms is more facile than that of those *trans* to the N atoms. The structure of this product is shown in Figure 8b (top, faster reaction). After 30 min of irradiation, three additional peaks are observed, labeled ‡ in Figure 8a, at 2.64, 2.47, and 1.97 ppm, believed to correspond to the product where one CH_3CN^N is substituted by D_2O (slower reaction, Figure 8b). The photochemistry of **7** is similar to that of **5**, although the formation of the aqua species is significantly slower for the former under similar experimental conditions, as indicated by the changes in the electronic and ^1H NMR spectra as a function of irradiation time (Supporting Information, Figure S18).

The quantum yields (Φ) for the ligand exchange were determined to be 0.030(6) for **5** and 0.0040(3) for **7** (λ_{irr} = 400 nm). These quantum yields were measured by monitoring the decrease in the absorption of the reactant at 550 nm as a function of irradiation time at early times; therefore, they correspond to the exchange of the eq CH_3CN ligand positioned *trans* to the O atom for one H_2O molecule. The value of Φ measured for **5** is comparable to that reported for *cis*-$[Rh_2(NHCOCH_3)_2(bpy)(CH_3CN)_2][BF_4]_2$, 0.04,[57] but is ~10-fold lower than that measured for H-T-*cis*-$[Rh_2(HNCOCH_3)_2(CH_3CN)_6][BF_4]_2$, 0.40,[34] in water. The value of Φ for **5**, however, is an order of magnitude greater than that of **7**. The H-H ligand arrangement of **7** is likely important in the observed photochemical properties, since the value of Φ measured for H-H *cis*-$[Rh_2(HNCOCH_3)_2(CH_3CN)_6][BF_4]_2$ is lower than that for the H-T isomer in water.[34]

Cellular Toxicity Studies. On the basis of the results from the photochemical investigations, complexes **5** and **7** were subjected to further cytotoxicity studies to test our hypothesis that the PCT potential exhibited by this family of dirhodium complexes is closely correlated to the photolability and dark stability of the eq CH_3CN ligands. Complex **4** was not investigated because of its instability in aqueous media (*vide supra*). The cellular toxicities of **5** and **7** against the HeLa cell line were determined both in the dark, IC_{50}^{Dark}, and upon visible light irradiation, IC_{50}^{Irr} ($\lambda_{irr} \geq 400$ nm), by SYTOX Green[58] and Hoechst 33342[59] assays. For the sake of comparison, the effect of visible light on the widely used chemotherapy agent cisplatin was also probed, and the detailed results are compiled in Table 3. The phototoxicity index (PI) values listed in Table 3 clearly show that **5** is superior to hematoporphyrin, a component in the PDT drug Photofrin.

Table 3. Cytotoxicity and Photocytotoxicity of Compounds 5 and 7, Determined from SYTOX Green and Hoechst 33342 Assays, and Their Comparisons with Cisplatin and Hematoporphyrin

	$IC_{50}^{Dark}/\mu M$	$IC_{50}^{Irr}/\mu M$	PI[a]
cisplatin	58 ± 4	47 ± 3	1.2[b]
hematoporphyrin	21 ± 1	3.8 ± 0.2	5.5[c]
5	630 ± 77	38.5 ± 9	16.4[b]
7	≫100	≫100	na

[a]PI = $IC_{50}^{Dark}/IC_{50}^{Irr}$. [b]Current study. [c]Ref 17g.

For the dark experiments, the HeLa cells were incubated with **5** and **7** for 2 h, followed by treatment with SYTOX Green and Hoechst 33342 dyes for 10 min. The cells incubated with **5** at a series of different concentrations (1, 10, 25, 50, and 75 μM) in the dark exhibit primarily blue fluorescence caused by the Hoechst 33342 nuclear stain, with no SYTOX Green staining being evident with the representative data collected on cells treated with a 50 μM concentration of **5** shown in Figure 9a–d, top panel. The absence of green fluorescence is indicative that the cells are not dead or dying, such that **5** is not toxic in the dark up to 75 μM, consistent with the measured IC_{50}^{Dark} value (Table 3). These results are similar to that observed for the control experiment where no compound is present (Supporting Information, Figure S19), an indication of very low toxicity for **5** in the dark. The LC_{50}^{Dark} value of **5** was determined to be 630 ± 77 μM, a value that is significantly higher than that of 58 ± 4 μM measured for cisplatin under similar experimental conditions (Table 3 and Supporting Information, Figure S20). The very low cytotoxicity of compound **5** in the dark is ascribed to the relative stability of its eq CH_3CN ligands in aqueous solution (*vide supra*). A significant increase in cell morbidity, however, is induced by **5** after irradiation of the cells for only 30 min (λ_{irr} > 400 nm) (bottom panel of Figure 9a–d). The LC_{50} value measured under irradiation conditions, LC_{50}^{Irr}, is 38.5 ± 9 μM, which is even lower than that of cisplatin. A phototoxicity index (PI) of $LC_{50}^{Dark}/LC_{50}^{Irr}$ = 16.4 was therefore calculated, which is much higher than the 5.5-fold increase for hematoporphyrin, which is a key component of the commercially available PDT agent Photofrin. The cause of the increase in cytotoxicity of **5** is ascribed to the facile generation of the active aqua species upon visible light irradiation (structural representation shown in Figure 8b), which is able to bind to the biomolecules in a fashion similar to that in cisplatin, as shown in our previous studies.[34,35] More importantly, complex **5** does not sensitize the production of $^1O_2$ owing to its short excited-state lifetime, 419 ps (Supporting Information, Figure S24), such that its photocytotoxicity is independent of O_2, rendering it a superior photochemotherapeutic agent for hypoxic tumors. These results show that a dose of compound **5** that is nontoxic in the dark could be activated upon irradiation of an area localized to the affected tissue. One issue, however, that one needs to bear in mind is that the light of $\lambda_{irr} \geq 400$ nm used in the present cell experiments with **5** is a result of the present output of the illumination box and may cause damage to normal cells upon longer light exposure times that otherwise can be avoided by the light used for the action of Photofrin, λ_{irr} = 630 nm. Complex **5**, however, absorbs light well into the PDT window, and solution experiments show that photoinduced ligand exchange remains operative with $\lambda_{irr} \geq 645$ nm, although it requires longer irradiation times (Supporting Information, Figure S25). It is therefore expected that illumination of **5** in the PDT window will also result in enhancement of toxicity upon irradiation.

In contrast, compound **7** does not exhibit enhanced cytotoxicity against the HeLa cancer cell line upon irradiation, as the data in Supporting Information, Figure S21 reveal, and, in fact, its LC_{50} values both in the dark and upon irradiation are estimated to be ≫100 μM (Figure S21). These results are not surprising, given the fact that the eq CH_3CN ligands are very inert to substitution in the dark, as well as the much lower quantum yield for generation of the aqua species upon visible light irradiation (*vide supra*).

dx.doi.org/10.1021/ja5078359 | J. Am. Chem. Soc. 2014, 136, 17058–17070

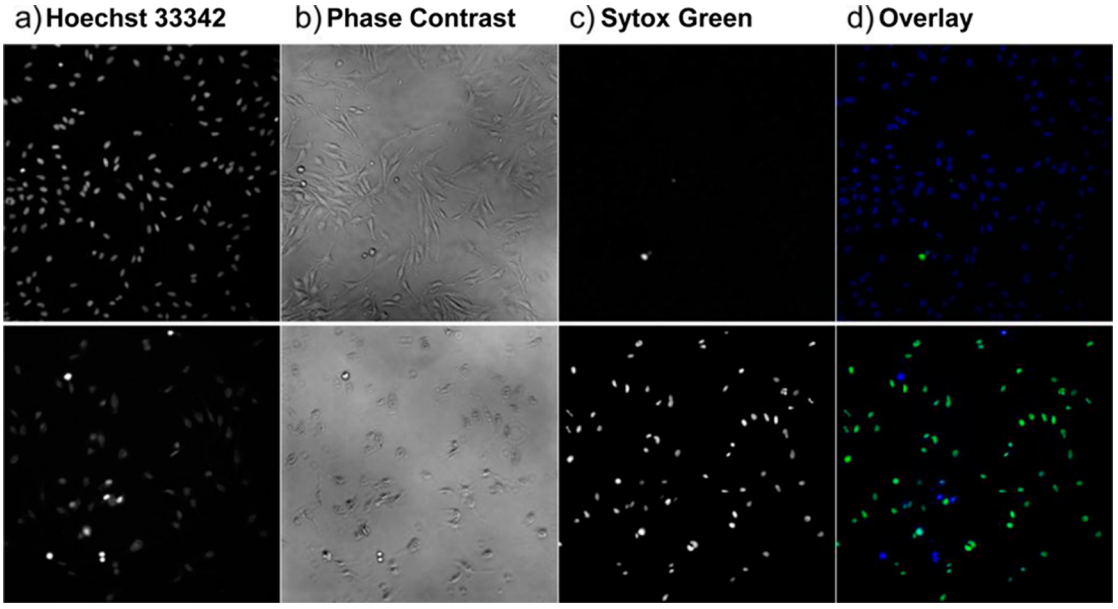

Figure 9. Confocal microscopy images of HeLa cells treated with 50 μM solutions of **5** followed by treatment with SYTOX Green and Hoechst, top panels in the dark and bottom panels irradiated: (a) Hoechst 33342 blue fluorescence, (b) phase contrast, (c) SYTOX Green fluorescence, and (d) overlay of blue and green fluorescence.

At this stage, we can conclude that the facile generation of the aqua species accounts for the cytotoxicity caused by this type of partial paddlewheel dirhodium complexes upon visible light irradiation, such as compound **5**. Furthermore, the relative stability of the eq CH_3CN ligands in the dark also plays an important role for optimal PCT properties, for which nontoxicity or low dark toxicity is achieved, e.g., compounds **5** and **7**. More importantly, the aforementioned two features, namely, photolability and dark stability of the eq CH_3CN ligands, can be readily accomplished through tuning the ligand field around the dimetal center by using an appropriate substituent on the bridging ligands, as demonstrated by compound **5** in the current study.

For the development of better photochemotherapeutic agents, another very important consideration is their induced cell death pathways, namely apoptosis or necrosis.[60] Given the fact that necrotic cells can cause severe inflammatory reactions,[61] most of the current clinically used anticancer drugs are based on apoptosis as the cell death pathway.[62] Dirhodium complexes developed jointly in our research groups were shown to be able to induce cell death via either apoptosis or necrosis, depending on the coordinated ligands.[63] Therefore, we conducted further biological assays to shed light on the cell death mechanism induced by compound **5**.

Mitochondria, essential for the synthesis of ATP and oxidative phosphorylation,[64,65] also play a critical role in the early stage of apoptotic cell death pathway via the release of cytochrome *c* as well as other apoptosis-inducing factors.[66] It has been proposed that the mitochondrial membrane potential ($\Delta\psi$) depletion is associated with the disruption of the mitochondrial membrane and marks early stages of apoptosis.[62] Therefore, the MitoProbe JC-1 (5′,6,6′-tetrachloro-1,1′,3,3′-tetraethylbenzimidazolylcarbocyanine iodide) assay was conducted on HeLa cells after treatment with compound **5** under visible light irradiation. The cationic JC-1 dye accumulates in the mitochondrial matrix, driven by an electrochemical gradient,[62,67] as indicated by a fluorescence emission shift from red ($\lambda_{max} \approx 590$ nm, hyperpolarized) to green ($\lambda_{max} \approx 525$ nm, depolarized).[65] In this vein, we conducted time- and concentration-dependent experiments with cationic JC-1 dye and monitored the changes in $\Delta\psi$ of the treated HeLa cells. The time lapse experiments reveal a consistent drop in $\Delta\psi$ after the treatment with **5**, and the representative cell images (20 μM **5**, taken at 1, 2, and 3 h, respectively) are displayed in Figure 10, in which a continuing decrease in the red fluorescence is clearly observed. The depletion in $\Delta\psi$ is achieved after a 3 h treatment, as indicated by the weak red fluorescence and very strong green stain. Furthermore, the concentration-dependent experiment (cell images taken at 1 h incubation time with 20, 50, and 75 μM **5**, respectively) indicates that the changes to $\Delta\psi$ are directly correlated with the dose of **5** (Supporting

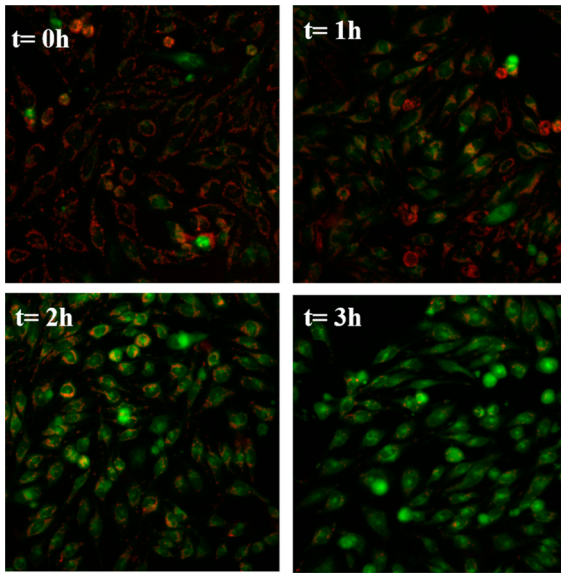

Figure 10. Time lapse fluorescence imaging of JC-1-labeled HeLa cells taken by confocal microscope after treatment with compound **5** at 20 μM.

dx.doi.org/10.1021/ja5078359 | J. Am. Chem. Soc. 2014, 136, 17058−17070

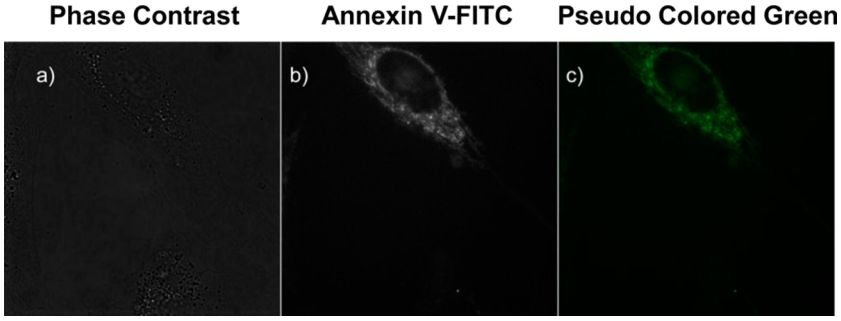

Figure 11. Confocal microscopy images of HeLa cells treated with 38.5 μM of **5** followed by treatment with Annexin V-FITC: (a) phase contrast image, (b) Annexin V-FITC green fluorescence, and (c) Annexin V-FITC pseudo-colored green image.

Information, Figure S22), indicating that the decrease in $\Delta\psi$ is indeed caused by compound **5**. The results lead to the conclusion that compound **5** induces HeLa cell death in a concentration- and time-dependent manner, which is indicative of the activation of mitochondria-mediated apoptosis.

In order to provide further evidence that compound **5** induces apoptosis-mediated cell death on HeLa cells, an Annexin V assay was also conducted. During apoptosis, different processes are activated in order to trigger the programmed cell death.[68] One of these is the exposure of phosphatidyl serine (PS) into the outer leaflet of the cell membrane.[69,70] Annexin V-FITC binds to PS that is exposed on the cell surface, which can then be monitored by cell fluorescence techniques. Cells treated with compound **5** and then irradiated exhibit green fluorescence (Figure 11b,c) localized on the outer side of the cellular membrane, which is indicative of PS on the outer leaflet of the membrane. The results obtained from the JC-1 dye and Annexin V-FTIX assays collectively point at an apoptotic cell death pathway caused by compound **5**.

CONCLUSIONS

A series of partial paddlewheel dirhodium complexes of general formula *cis*-$[Rh_2(xhp)_2(CH_3CN)_n][BF_4]_2$ (xhp = mhp, chp, and fhp, n = 5 or 6) were synthesized and fully characterized by single-crystal X-ray diffraction and ^{1}H NMR spectroscopy. The equatorial CH_3CN ligands in this family of compounds were determined to be kinetically labile upon dissolution in CH_3CN and H_2O in the dark, as indicated by the ^{1}H NMR and electronic spectroscopic studies. Importantly, the lability of the eq CH_3CN ligands can be tuned through judicious choice of the substituents on the bridging ligands. Specifically, the ligand lability decreases in the order mhp > chp > fhp, which is in agreement with the hypothesis that the more electron donating ligands exert stronger *trans* effects. The irradiation of **5** in water with visible light leads to the exchange of one eq CH_3CN ligand for a solvent H_2O molecule. Similar photoreactivity is observed for **7**, but the degradation products are formed at lower concentrations due to the lower electron donating nature of the bridging fhp ligands. This finding is in good agreement with the results of SYTOX Green assays, which revealed that compound **5** holds great potential as a photochemotherapy anticancer agent, owing to a 16.4-fold increase in cytotoxicity against HeLa cell lines upon visible light irradiation, and is much more toxic than cisplatin upon light irradiation. The mechanism of HeLa cell death induced by **5** upon irradiation was determined to be apoptosis using JC-1 dye and Annexin V-FITC assays, which is a desired outcome. The current study underscores the importance of tuning the ligand field around the Rh_2(II,II) centers to achieve dark stability and to concomitantly increase photolability of the eq CH_3CN ligands to optimize photochemotherapeutic action. Ongoing experiments include elucidation of the specific cellular targets and organelles, the results of which will be reported in due course.

ASSOCIATED CONTENT

Supporting Information

^{1}HNMR spectra for **1**, **2**, and **4**−**7**; crystal data for **1** and **3**−**6**; ^{1}HNMR spectral changes for **4**, **5**, and **7** in CD_3CN and in D_2O in the dark; additional data from calculations; and photolysis data for **7**. This material is available free of charge via the Internet at http://pubs.acs.org. CCDC files 998901 (**4**), 998900 (**5**), and 998899 (**6**) contain the supplementary crystallographic data for this paper and can be obtained free of charge from The Cambridge Crystallographic Data Centre via www.ccdc.cam.ac.uk/data_request/cif.

AUTHOR INFORMATION

Corresponding Authors

pellois@tamu.edu
turro.1@osu.edu
dunbar@mail.chem.tamu.edu

Author Contributions

$^\perp$Z.L. and A.D. contributed equally.

Notes

The authors declare no competing financial interest.

ACKNOWLEDGMENTS

C.T. thanks the Department of Energy Basic Energy Sciences (DE-SC0010542) for partial support of this work in the form of salary for B.A. K.R.D. thanks the Welch Foundation (A-449) for summer salary for Z.L. The authors gratefully acknowledge the Super Computing Facility and the Laboratory for Molecular Simulation (National Science Foundation CHE-0541587) at Texas A&M University for providing software and computer time. C.T. thanks the Center for Chemical and Biophysical Dynamics (CCBD) at Ohio State for ultrafast laser measurements.

REFERENCES

(1) (a) Rosenberg, B.; Van Camp, L.; Krigas, T. *Nature* **1965**, *205*, 698−699. (b) Rosenberg, B.; Van Camp, L.; Trosko, J. E.; Mansour, V. H. *Nature* **1969**, *222*, 385−386.

(2) (a) Dhar, S.; Lippard, S. J. Current Status and Mechanism of Action of Platinum-Based Anticancer Drugs. In *Bioinorganic Medicinal Chemistry*; Alessio, E., Ed.; Wiley-VCH: Weinheim, 2010; pp 79−86.

(b) Ang, W. H.; Myint, M. N. Z.; Lippard, S. J. *J. Am. Chem. Soc.* **2010**, *132*, 7429−7435. (c) Todd, R. C.; Lippard, S. J. *J. Inorg. Biochem.* **2010**, *104*, 902−908. (d) Kelland, L. *Nat. Rev. Cancer* **2007**, *7*, 573−584. (e) Jung, Y.; Lippard, S. J. *Chem. Rev.* **2007**, *107*, 1387−1407. (f) Mantri, Y.; Lippard, S. J.; Baik, M. H. *J. Am. Chem. Soc.* **2007**, *129*, 5023−5030. (g) Wang, D.; Lippard, S. J. *Nat. Rev. Drug Discovery* **2005**, *4*, 307−320. (h) Jamieson, E. R.; Lippard, S. J. *Chem. Rev.* **1999**, *99*, 2467−2498. (i) Zamble, D. B.; Lippard, S. J. *Trends Biochem. Sci.* **1995**, *20*, 435−439.

(3) *Cisplatin: Chemistry and Biochemistry of a Leading Anticancer Drug*; Lippert, B., Ed.; Wiley-VCH: Wurzburg, Germany, 1999.

(4) *Platinum-Based Drugs in Cancer Therapy*; Kelland, L. R., Farell, N., Eds.; Humana: Totowa, NJ, 2000.

(5) Rajski, S. R.; Williams, R. M. *Chem. Rev.* **1998**, *98*, 2723−2795.

(6) (a) Cohen, S. M.; Lippard, S. J. *Prog. Nucleic Acid Res. Mol. Biol.* **2001**, *67*, 93−130. (b) Zhang, C. X.; Lippard, S. J. *Curr. Opin. Chem. Biol.* **2003**, *7*, 481−489.

(7) (a) Fuertes, M. A.; Alonso, C.; Perez, J. M. *Chem. Rev.* **2003**, *103*, 645−662. (b) Fuertes, M. A.; Castilla, J.; Alonso, C.; Perez, J. M. *Curr. Med. Chem.: Anti-Cancer Agents* **2002**, *2*, 539−551.

(8) (a) Siddik, Z. H. *Cancer Treat. Res.* **2002**, *112*, 263−284. (b) Siddik, Z. H. *Oncogene* **2003**, *22*, 7265−7279.

(9) (a) Calvert, A. H.; Harland, S. J.; Newell, D. R.; Siddik, Z. H.; Jones, A. C.; McElwain, T. J.; Raju, S.; Wiltshaw, E.; Smith, I. E.; Baker, J. M.; Peckham, M. J.; Harrap, K. R. *Cancer Chemother. Pharmacol.* **1982**, *9*, 140−147. (b) Evans, B. D.; Raju, K. S.; Calvert, A. H.; Harland, S. J.; Wiltshaw, E. *Cancer Treat. Rep.* **1983**, *67*, 997−1000.

(10) Raymond, E.; Faivre, S.; Chaney, S.; Woynarowski, J.; Cvitkovic, E. *Mol. Cancer Ther.* **2002**, *1*, 227−235.

(11) Di Francesco, A. M.; Ruggiero, A.; Riccardi, A. *Cell. Mol. Life Sci.* **2002**, *59*, 1914−1927.

(12) Wheate, N. J.; Walker, S.; Craig, G. E.; Oun, R. *J. Chem. Soc., Dalton Trans.* **2010**, *39*, 8113−8127.

(13) (a) Hope, J. M.; Wilson, J. J.; Lippard, S. J. *J. Chem. Soc., Dalton Trans.* **2013**, *42*, 3176−3180. (b) Wilson, J. J.; Lippard, S. J. *Inorg. Chem.* **2012**, *51*, 9852−9864. (c) Park, G. Y.; Wilson, J. J.; Song, Y.; Lippard, S. J. *Proc. Natl. Acad. Sci. U.S.A.* **2012**, *109*, 11987−11992. (d) Wilson, J. J.; Lippard, S. J. *J. Med. Chem.* **2012**, *55*, 5326−5336. (e) Zhu, G.; Myint, M.; Ang, W. H.; Song, L.; Lippard, S. J. *Cancer Res.* **2012**, *72*, 790−800. (f) Lovejoy, K.; Serova, M.; Bieche, I.; Emami, S.; D'Incalci, M.; Broggini, M.; Erba, E.; Gespach, C.; Cvitkovic, E.; Faivre, S.; Raymond, E.; Lippard, S. J. *Mol. Cancer Ther.* **2011**, *10*, 1709−1719. (g) Wilson, J. J.; Lippard, S. J. *Inorg. Chem.* **2011**, *50*, 3103−3115. (h) Johnstone, T. C.; Wilson, J. J.; Lippard, S. J. *Inorg. Chem.* **2013**, *52*, 12234−12249. (i) Wilson, J. J.; Lippard, S. J. *Chem. Rev.* **2014**, *114*, 4470−4495. (j) Johnstone, T. C.; Lippard, S. J. *J. Am. Chem. Soc.* **2014**, *136*, 2126−2134.

(14) (a) Varbanov, H.; Valiahdi, S. M.; Legin, A. A.; Jakupec, M. A.; Roller, A.; Galanski, M.; Keppler, B. K. Eur. *J. Med. Chem.* **2011**, *46*, 5456−5464. (b) Reithofer, M. R.; Bytzek, A. K.; Valiahdi, S. M.; Kowol, C. R.; Groessl, M.; Hartinger, C. G.; Jakupec, M. A.; Galanski, M.; Keppler, B. K. *J. Inorg. Biochem.* **2011**, *105*, 46−51. (c) Scaffidi-Domianello, Y. Y.; Meelich, K.; Jakupec, M. A.; Arion, V. B.; Kukushkin, V. Y.; Galanski, M.; Keppler, B. K. *Inorg. Chem.* **2010**, *49*, 5669−5678.

(15) (a) Mangrum, J. B.; Farrell, N. P. *Chem. Commun.* **2010**, *46*, 6640−6650. (b) Gwak, H.-S.; Shingu, T.; Chumbalkar, V.; Hwang, Y.-H.; DeJournett, R.; Latha, K.; Koul, D.; Yung, W. K.; Powis, G.; Farrell, N. P.; Bögler, O. *Int. J. Cancer* **2010**, *128*, 787−796.

(16) (a) Ma, G.; Min, Y.; Huang, F.; Jiang, T.; Liu, Y. *Chem. Commun.* **2010**, *46*, 6938−6940. (b) Li, C.; Li, Z.; Sletten, E.; Arnesano, F.; Losacco, M.; Natile, G.; Liu, Y. *Angew. Chem., Int. Ed.* **2009**, *48*, 8497−8500.

(17) (a) Chifotides, H. T.; Dunbar, K. R. *J. Am. Chem. Soc.* **2007**, *129*, 12480−12490. (b) Kang, M.; Chouai, A.; Chifotides, H. T.; Dunbar, K. R. *Angew. Chem., Int. Ed.* **2006**, *45*, 6148−6151. (c) Kang, M.; Chifotides, H. T.; Dunbar, K. R. *Biochemistry* **2008**, *47*, 2265−2276. (d) Aguirre, J. D.; Chifotides, H. T.; Angeles-Boza, A. M.; Chouai, A.; Turro, C.; Dunbar, K. R. *Inorg. Chem.* **2009**, *48*, 4435−4444. (e) Angeles-Boza, A. M.; Chifotides, H. T.; Aguirre, J. D.; Chouai, A.; Fu, P. K.-L.; Dunbar, K. R.; Turro, C. *J. Med. Chem.* **2006**, *49*, 6841−6847. (f) Chifotides, H. T.; Dunbar, K. R. *Acc. Chem. Res.* **2005**, *38*, 146−156 and references therein. (g) Angeles-Boza, A. M.; Bradley, P. M.; Fu, P. K.-L.; Shatruk, M.; Hilfiger, M. G.; Dunbar, K. R.; Turro, C. *Inorg. Chem.* **2005**, *44*, 7262−7264.

(18) (a) Li, Z.; Shtemenko, N. I.; Yegorova, D. Y.; Babiy, S. O.; Brown, A. J.; Yang, T.; Shtemenko, A. V.; Dunbar, K. R. *J. Liposome Res.* **2014**, DOI: 10.3109/08982104.2014.954127. (b) Shtemenko, N. I.; Chifotides, H. T.; Domasevitch, K. V.; Golichenko, A. A.; Babiy, S. A.; Li, Z.; Paramonova, K. V.; Shtemenko, A. V.; Dunbar, K. R. *J. Inorg. Biochem.* **2013**, *129*, 127−134. (c) Shtemenko, A. V.; Collery, P.; Shtemenko, N. I.; Domasevitch, K. V.; Zabitskayac, E. D.; Golichenkoa, A. A. *Dalton Trans.* **2009**, 5132−5136.

(19) (a) Chatterjee, S.; Kundu, S.; Bhattacharyya, A.; Hartinger, C. G.; Dyson, P. J. *J. Biol. Inorg. Chem.* **2008**, *13*, 1149−1155. (b) Ang, W. H.; Casini, A.; Sava, G.; Dyson, P. J. *J. Organomet. Chem.* **2011**, *696*, 989−998. (c) Kilpin, K. J.; Clavel, C. M.; Edafe, F.; Dyson, P. J. *Organometallics* **2012**, *31*, 7031−7039. (d) Suntharalingam, K.; Johnstone, T. C.; Bruno, P. M.; Lin, W.; Hemann, M. T.; Lippard, S. J. *J. Am. Chem. Soc.* **2013**, *135*, 14060−14063.

(20) Celli, J. P.; Spring, B. Q.; Rizvi, I.; Evans, C. L.; Samkoe, K. S.; Verma, S.; Pogue, B. W.; Hasan, T. *Chem. Rev.* **2010**, *110*, 2795−2838.

(21) Allison, R. R.; Sibata, C. H. *Photodiagn. Photodyn. Ther.* **2010**, *7*, 61−75.

(22) Wolkenberg, S. E.; Boger, D. L. *Chem. Rev.* **2002**, *102*, 2477−2496.

(23) Dougherty, T. J.; Gomer, C. J.; Henderson, B. W.; Jori, G.; Kessel, D.; Korbelik, M.; Moan, J.; Peng, Q. *J. Natl. Cancer Inst.* **1998**, *90*, 889−905.

(24) Dolmans, D. E.; Fukumura, D.; Jain, R. K. *Nat. Rev. Cancer* **2003**, *3*, 380−387.

(25) DeRosa, M. C.; Crutchley, R. J. *Coord. Chem. Rev.* **2002**, *233*−*234*, 351−371.

(26) Harris, A. L. *Nat. Rev. Cancer* **2002**, *2*, 38−47.

(27) Shannon, A. M.; Bouchier-Hayes, D. J.; Condron, C. M.; Toomey, D. *Cancer Treat. Rev.* **2003**, *29*, 297−307.

(28) Guppy, M. *Biochem. Biophys. Res. Commun.* **2002**, *299*, 676−680.

(29) (a) Westendorf, A. F.; Zerzankova, L.; Salassa, L.; Sadler, P. J.; Brabec, V.; Bednarski, P. J. *J. Inorg. Biochem.* **2011**, *105*, 652−662. (b) Ronconi, L.; Sadler, P. J. *J. Chem. Soc., Dalton Trans.* **2011**, *40*, 262−268. (c) Liu, H.-K.; Sadler, P. J. *Acc. Chem. Res.* **2011**, *44*, 348−359. (d) Farrer, N. J.; Woods, J. A.; Salassa, L.; Zhao, Y.; Robinson, K. S.; Clarkson, G.; Mackay, F. S.; Sadler, P. J. *Angew. Chem., Int. Ed.* **2010**, *49*, 8905−8908. (e) Salassa, L.; Ruiu, T.; Garino, C.; Pizarro, A. M.; Bardelli, F.; Gianolio, D.; Westendorf, A.; Bednarski, P. J.; Lamberti, C.; Gobetto, R.; Sadler, P. J. *Organometallics* **2010**, *29*, 6703−6710. (f) Farrer, N. J.; Woods, J. A.; Munk, V. P.; Mackay, F. S.; Sadler, P. J. *Chem. Res. Toxicol.* **2010**, *23*, 413−421. (g) Farrer, N. J.; Salassa, L.; Sadler, P. J. *J. Chem. Soc., Dalton Trans.* **2009**, *48*, 10690−10701. (h) Betanzos-Lara, S.; Salassa, L.; Habtemariam, A.; Novakova, O.; Pizarro, A. M.; Clarkson, G. J.; Liskova, B.; Brabec, V.; Sadler, P. J. *Organometallics* **2012**, *31*, 3466−3479. (i) Zhao, Y.; Roberts, G. M.; Greenough, S. E.; Farrer, N. J.; Paterson, M. J.; Powell, W. H.; Stavros, V. G.; Sadler, P. J. *Angew. Chem., Int. Ed.* **2012**, *51*, 11263−11266. (j) Butler, J. S.; Woods, J. A.; Farrer, N. J.; Newton, M.E.; Sadler, P. J. *J. Am. Chem. Soc.* **2012**, *134*, 16508−16511. (k) Zhao, Y.; Farrer, N. J.; Li, H. L.; Butler, J. S.; McQuitty, R. J.; Habtemariam, A.; Wang, F. Y.; Sadler, P. J. *Angew. Chem., Int. Ed.* **2013**, *52*, 13633−13637.

(30) (a) Higgins, S. L. H.; Brewer, K. J. *Angew. Chem., Int. Ed.* **2012**, *51*, 11420−11422. (b) Wachter, E.; Heidary, D. K.; Howerton, B. S.; Parkin, S.; Glazer, E. C. *Chem. Commun.* **2012**, *48*, 9649−9651.

(31) Respondek, T.; Garner, R. N.; Herroon, M. K.; Podgorski, I.; Turro, C.; Kodanko, J. J. *J. Am. Chem. Soc.* **2011**, *133*, 17164−17167.

(32) Garner, R. N.; Joyce, L. E.; Turro, C. *Inorg. Chem.* **2011**, *50*, 4384−4391.

(33) Sgambellone, M. A.; David, A.; Garner, R. N.; Dunbar, K. R.; Turro, C. *J. Am. Chem. Soc.* **2013**, *135*, 11274−11282.

(34) Lutterman, D. A.; Fu, P. K.-L.; Turro, C. *J. Am. Chem. Soc.* **2006**, *128*, 738−739.
(35) Burya, S. J.; Palmer, A. M.; Galucci, J. C.; Turro, C. *Inorg. Chem.* **2012**, *51*, 11882−11890.
(36) Li, Z.; Burya, S. J.; Turro, C.; Dunbar, K. R. *Philos. Trans. R. Soc. A* **2013**, *371*, No. 20120128.
(37) Rempel, G. A.; Legzdins, P.; Smith, H.; Wilkinson, G. *Inorg. Synth.* **1971**, *13*, 90−91.
(38) Cotton, F. A.; Felthouse, T. R. *Inorg. Chem.* **1981**, *20*, 584−600.
(39) Monalti, M.; Credi, A.; Prodi, L.; Gandolfi, M. T. *Handbook of Photochemistry*, 3rd ed.; Taylor & Francis Group: Boca Raton, FL, 2006; pp 601−616.
(40) Frisch, M. J. et al. *Gaussian 09*, Revision B.01; Gaussian Inc.: Wallingford, CT, 2010 (the full list of authors can be found in the Supporting Information).
(41) (a) Adamo, C.; Barone, V. *J. Chem. Phys.* **1998**, *108*, 664−675. (b) Perdew, J. P.; Chevary, J. A.; Vosko, S. H.; Jackson, K. A.; Pederson, M. R.; Singh, D. J.; Fiolhais, C. *Phys. Rev. B* **1992**, *46*, 6671−6687. (c) Perdew, J. P.; Burke, K.; Wang, Y. *Phys. Rev. B* **1996**, *54*, 16533−16539.
(42) Dolg, M.; Stoll, H.; Preuss, H.; Pitzer, R. M. *J. Phys. Chem.* **1993**, *97*, 5852−5859.
(43) (a) Petersson, G. A.; Bennett, A.; Tensfeldt, T. G.; Allaham, M. A.; Shirley, W. A.; Mantzaris, J. *J. Chem. Phys.* **1988**, *89*, 2193−2218. (b) Petersson, G. A.; Allaham, M. A. *J. Chem. Phys.* **1991**, *94*, 6081−6090.
(44) (a) Bauernschmitt, R.; Ahlrichs, R. *Chem. Phys. Lett.* **1996**, *256*, 454−464. (b) Casida, M. E.; Jamorski, C.; Casida, K. C.; Salahub, D. R. *J. Chem. Phys.* **1998**, *108*, 4439−4449. (c) Stratmann, R. E.; Scuseria, G. E.; Frisch, M. J. *J. Chem. Phys.* **1998**, *109*, 8218−8224. (d) Van Caillie, C.; Amos, R. D. *Chem. Phys. Lett.* **1999**, *308*, 249−255. (e) Van Caillie, C.; Amos, R. D. *Chem. Phys. Lett.* **2000**, *317*, 159−164. (f) Furche, F.; Ahlrichs, R. *J. Chem. Phys.* **2002**, *117*, 7433−7447. (g) Scalmani, G.; Frisch, M. J.; Mennucci, B.; Tomasi, J.; Cammi, R.; Barone, V. *J. Chem. Phys.* **2006**, *124*, 1−15.
(45) (a) Tomasi, J.; Mennucci, B.; Cammi, R. *Chem. Rev.* **2005**, *105*, 2999−3093. (b) Tomasi, J. In *Structure and Reactivity in Aqueous Solution*; Cramer, C. J.; Truhlar, D. G., Eds.; ACS Symposium Series *568*; American Chemical Society: Washington, DC, 1994; pp 10−23.
(46) Dennington, R. D., II; Keith, T. A.; Millam, J. M. *Agui 9.2.1*; Semichem, Inc.: Shawnee Mission, KS, 2008.
(47) *SAINT*, Program for area detector absorption correction; Siemens Analytical X-Ray Instruments Inc.: Madison, WI, 1994−1996.
(48) Sheldrick, G. M. *SADABS*, Program for Siemens area detector absorption correction; University of Göttingen: Göttingen, Germany, 1996.
(49) (a) Barbour, L. J. *X-Seed*, Graphical interface to SHELX-97 and POV-Ray, 1999; http://www.ccp14.ac.uk/ccp/web-mirrors/x-seed/index.html. (b) Barbour, L. J. *J. Supramol. Chem.* **2001**, *1*, 189−191. (c) Atwood, J. L.; Barbour, L. J. *Cryst. Growth Des.* **2003**, *3*, 3−8.
(50) Sheldrick, G. M. *Acta Crystallogr., Sect. A* **2008**, *A64*, 112−122.
(51) Latt, S. A.; Stetten, G. *J. Histochem. Cytochem.* **1976**, *24*, 24−33.
(52) Latt, S. A. *J. Histochem. Cytochem.* **1977**, *25*, 913−926.
(53) Cotton, F. A.; Han, S.; Wang, W. *Inorg. Chem.* **1984**, *23*, 4762−4765.
(54) Li, Z.; Chifotides, H. T.; Dunbar, K. R. *Chem. Sci.* **2013**, *4*, 4470−4485.
(55) Li, Z.; Leed, N. A.; Dickson-Karn, N. M.; Dunbar, K. R.; Turro, C. *Chem. Sci.* **2014**, *5*, 727−737.
(56) Chifotides, H. T.; Dunbar, K. R. Rhodium Compounds. In *Multiple Bonds Between Metal Atoms*, 3rd ed.; Cotton, F. A., Murillo, C., Walton, R. A., Eds.; Springer-Science and Business Media, Inc.: New York, 2005; Chap. 12, pp 465−589.
(57) Palmer, A. M.; Burya, S. J.; Gallucci, J. C.; Turro, C. *Chem. Med. Chem.* **2014**, *9*, 1260−1265.
(58) SYTOX Green Nucleic Acid Stain. *The Molecular Probes Handbook*; Invitrogen, 2007.
(59) Hoechst Stains. *The Molecular Probes Handbook*; Life Technologies, 2005.
(60) Vermes, I.; Haanen, C. *Adv. Clin. Chem.* **1984**, *31*, 177−246.
(61) Thornberry, N. A.; Lazebnik, Y. *Science* **1998**, *281*, 1312−1316.
(62) Ghobrial, I. M.; Witzig, T. E.; Adjei, A. A. *Ca-Cancer J. Clin.* **2005**, *55*, 178−194.
(63) Aguirre, J. D.; Angeles-Boza, A. M.; Chouai, A.; Turro, C.; Pellois, P.; Dunbar, K. R. *Dalton Trans.* **2009**, *48*, 10806−10812.
(64) Singh, K. *Mitochondrial DNA Mutations in Aging, Disease, and Cancer*; Springer: New York, 1998; pp 147−165.
(65) Gottlieb, R. *Biol. Signals Recept.* **2001**, *10*, 147.
(66) Hengartner, M. O. *Nature* **2000**, *407*, 770−776.
(67) Nowak, G. Y. *J. Biol. Chem.* **2002**, *277*, 43377.
(68) Brady, H. J. M. *Apoptosis Methods and Protocols*; Humana Press: Totowa, NJ, 2004; Vol. *282*.
(69) Telford, W.; Komoriya, A.; Packard, B. In *Flow Cytometry Protocols*; Hawley, T., Hawley, R., Eds.; Humana Press: Totowa, NJ, 2004; Vol. *263*, p 141.
(70) Lee, S. H.; Meng, X. W.; Flatten, K. S.; Loegering, D. A.; Kaufmann, S. H. *Cell Death Differ.* **2012**, *20*, 64.